Numerical Investigation and Performance Evaluation of Food Grain Drying Unit Integrated with the Thermal Energy Storage System

Ashutosh Verma[1], Rajeev Kukreja[1], Srinivas Tangellapalli[1],Dharam Buddhi[2]

[1]Dr. B. R. Ambedkar National Institute of Technology Jalandhar, Punjab (India)
[2]Uttranchal University Dehradun, Uttarakhand (India)

Abstract

In this work, the numerical study of a 10kW thermal energy storage (TES) system is conducted in order to facilitate the solar drying unit and to evaluate its potential. A drying chamber, a solar air collector, and a thermal energy storage system utilizing Phase Change Material (PCM) as a storage medium built up the investigated solar drying unit (SDU). The numerical model of the thermal energy storage system integrated with the drying unit is used to evaluate the potential of the solar dryer. The medium-range commercial-grade PCM X-180 is used for thermal energy storage purposes. The effect of various parameters on thermal energy storage (TES) and drying performance at various mass flow rates is evaluated. The results of this analysis show that the proposed design of SDU is worthy and promising since it utilizes renewable energy and reports savings between 30 to 70 % in operating cost for varying TES capacities and unit configuration.

Keywords: *Thermal energy storage, phase change material, solar drying unit, renewable energy*

1. Introduction

The drying process of agricultural commodities is essential for their preservation. Especially the drying process of pulses and grains requires a flow of hot air inside the dryer within the temperature range of 70-75ºC. To ensure the quality of the product while storage it is required to reduce the moisture content below 15ºC. A survey has been conducted for the collection of data from various food processing industries and the essential input and operational parameters of conventional grain/pulses dryer are used in this work. The conventional dryers used in process industries operate on electricity, fossil fuels, or biomass which in turn produces toxic gasses. Many of the researchers conducted an experimental study on the solar air dryer integrated with thermal energy storage (TES) for improving its efficiency, cost-effectiveness, and reducing carbon emission. Saeed Mehrana et.al [1] conducted an experimental study on a fluidized-bed dryer assisted with a solar water heater and solar powdered infrared lamp. The gas water heater used in the absence of solar energy produces a uniform drying temperature of 35 ºC and 45 ºC. The maximum energy required for the drying of rice paddy grains is 1.163kWh at the air velocity of 9m/s and drying temperature of 55ºC and 0.314kWh and air velocity of 7m/s and drying temperature of 45 ºC. The limitations with such types of dryers are less energy storage capacity due to sensible heat storage and reduced drying operation time in the absence of sunlight. However, the use of sensible storage maintains the moderate drying temperature which is the essential requirement for a quality outcome. Halil [2] conducted an experiment on the solar dryer equipped with packed bed TES used for the drying of 5 mm thick orange slices, reduces the moisture content from 93.5% to 10.28%. The exergy assessment reports the improvement of thermal efficiency of dryer, in case of using TES from 58.7% to 68.4% by the author. The average value of useful energy consumed during two set of experiments are 89.8MJ and 88.1 MJ respectively. The unavailability of solar energy in night and variation in solar radiations in day time promotes the use of TES to maintain the thermal stability and improve the drying performance and dryer efficiency. The Bilal et.al [3] conduct the numerical investigation on hybrid electric-solar dryer for food integrated with TES. These studies mostly involve the use of phase change material (PCM) suitable for sensible heat storage and low temperature latent heat storage materials with low melting point. The use of medium high temperature PCM in TES technology is the gap in literature. The present work is the theoretical model and its numerical simulation for the use of medium range PCMs in solar energy storage technologies used for drying grains/pulses.

doi:10.18086/eurosun.2022.13.23 Available at http://proceedings.ises.org

2. Material and method

The thermal performance and drying quality of the theoretically designed solar-drying unit (SDU) integrated with thermal energy storage (TES) have been examined in this study. Fig. 1 shows the schematic layout of the SDU and its main components (Solar collector, solar receiver, solar thermal energy storage, and air-drying chamber integrated with radiator type heat exchanger).

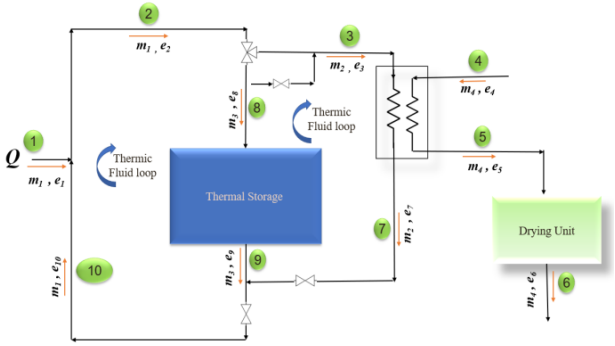

Fig. 1: Schematic layout of the solar drying unit

The solar radiation collected at the collector of 16m^2 of Scheffler dish is focused on the receiver, and transferred to the HTF passes through it. Operational parameters of the experimental investigation conducted by Dnyaneshwar Malwad [4] with the improved design of convex receiver with 68.4% of energy efficiency have been used under this study. Considering the solar radiation collected from three scheffler dishes this study is being carried out further for charging TES and drying pluses/grains. Thermophysical properties of heat transfer fluid (HTF) Thermenol 66 [5] and commercial grade PCM X-180 is used for this study, reported in table 1. The system is designed to operate in the dual-mode, wherein daytime direct drying allows the SDU to operate independently, while the TES supplies the essential energy during sunset (night). The pulses dryer facilitated with the radiator allows exchanging heat from the HTF to air, the working fluid in the pulse's dryer. The air coming from the outside passes through the radiator heat exchanger, where it heats up and then leads the drying unit to dry pulses. The thermic fluid pump of 0.75 kW and 0.5 kW air blower of calculated capacity are utilized to circulate HTF in closed-loop and air inside solar dryer, respectively. The thermophysical properties of commercial grade PCM X180 of company EPL ltd are used for this study[6] reported in Tab. 1.

Tab. 1: Thermophysical properties of PCM and encapsulation material

Material	Density (kg/m^3)	K (W/m-K)	Temperature (°C)		Latent heat (kJ/kg)	Specific heat (kJ/kg-K)
PCM X180	1330	0.36	Solid	179	280	1.4
			Liquid	180		
Aluminum	2719	202.4	--		--	8.71

3. System Design

3.1 Thermal Energy Storage (TES)

The availability of thermal energy storage of parabolic solar concentrators is the most distinctive, cost-effective, and resilient in the area of solar grain drying. The effective usage of a PCM depends on designing a device that offers adequate encapsulation for the PCM and a container for the heat transfer fluid (HTF). The geometric design of the storage system is critical for improving heat transfer rates and, as a result, for the improvement of latent heat thermal energy storage (LHTES) technology. A typical PCM-based TES device generally consists of components that can only work when incorporated into a system. Cascade arrangement of plates inside TES tanks for storing solar thermal energy utilizing PCM are technically and economically more advantageous[7]. Fig. 2 shows the configuration of plates inside the TES tank. Two distinct TES modules, one with fins and the other without fins, are used to examine the performance of the solar drying unit.

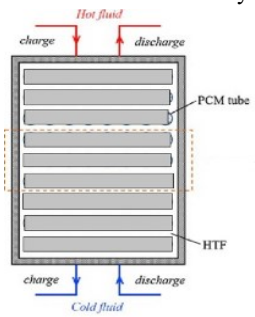

Fig. 2: Plates arrangements inside thermal energy storage (TES) tank

The hydrodynamic study is performed to determine, the gap of 2mm allow to flow HTF, between two slabs of thickness 50 mm. The one-dimensional heat flow model is derived to calculate the optimum heat transfer area and, subsequently, the fins required for the heat transfer.

3.2 Design of drying unit

The operational parameters of a continuous batch dryer of a capacity 20kg/batch are used to investigate the drying performance. The radiator-type heat exchanger of 4 kW, 0.45 effectiveness, and 6.3 m^2 of calculated area for exchanging heat from HTF to air is used[8]. The air blower of 0.75 kW forced the air at 0.21kg/s and temperature 75^{o}C inside the dryer, reducing the moisture content from 14 to 4% in 45 minutes. The energy required for drying can be calculated using eq. 1, where M is the mass of feed, C_p is the specific heat in kJ/kg-K, MR is moisture ratio, and λ is latent heat in kJ/kg.

$$E_d = Mc_p(T_f - T_i) + MR.\lambda \qquad \text{(eq. 1)}$$

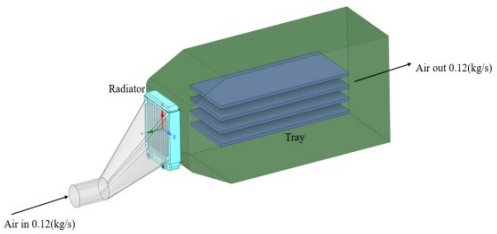

Fig. 3: Isometric view of the drying unit

4. Numerical approach

A 2D CFD dynamic model for the TES module with fin is developed using ANSYS® Fluent shown in Fig. 4. The CFD model is used to investigate the impacts of various HTF flow rates on the melting and solidification processes

of the TES and drying performance of the system. The UDF is interrupt to define HTF and PCM properties and standard k-ε turbulence model with standard wall function is selected. For the coupling of pressure and velocity, the Semi-Implicit Method for Pressure Linked Equations (SIMPLE) is used. The momentum and energy equations of the model are discretized using a second-order upwind method. The pressure staggering option (PRESTO) scheme used for the pressure correction equation. For pressure, density, body forces, momentum, liquid fraction, and energy, the relaxation factors are 0.3, 1.0, 1.0, 0.7, 0.9, and 1.0, respectively. To confirm convergence at each time step, the residual requirements are set to 10^6 for the continuity and momentum equations, and 10^9 for the energy equation.

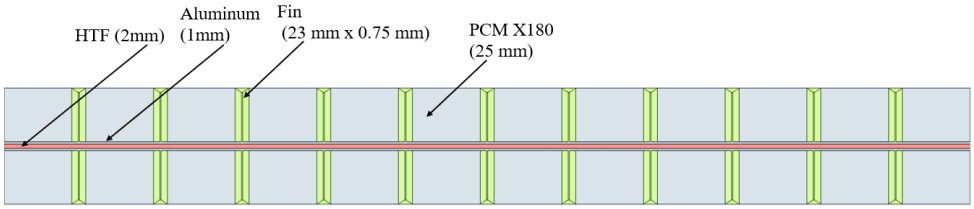

Fig. 4: 2D model for the numerical study

4.1 Governing Equation

To conduct the computation of three physical processes has been considered i.e.

I. Fluid flow modeling.
II. Conductive heat transfer.
III. Convective heat transfer.

4.2 Fluid flow modeling

The continuity equation along with Navier–Stokes equation need to be solved concurrently to mathematically model the dynamic behavior of the HTF flowing inside channel. The continuity equation is written as eq. 2:

$$\frac{\partial \rho_f}{\partial t} + \vec{\nabla} \cdot \left(\rho_f \vec{v} \right) = 0 \qquad \text{(eq. 2)}$$

Where v is the velocity and ρ_f is the density of the HTF. The N-S equation in cartesian coordinates, which accounts for momentum conservation, is given as eq. 3.

$$\rho_f \frac{D\rho_f}{Dt} = -\vec{\nabla} P + \mu \nabla^2 \vec{v} = 0 \qquad \text{(eq. 3)}$$

Where, P is the dynamic pressure term of the fluid field and μ is the dynamic viscosity of the HTF.

4.3 Conductive heat transfer: solid region

Conduction heat transfers from the HTF channel side walls to PCM must be solved using heat conduction eq. 4.

$$\rho_s C_{ps} \frac{\partial T}{\partial t} = k_s \nabla^2 T \qquad \text{(eq. 4)}$$

4.4 Convective heat transfer: solid to fluid region

Convective heat transfer from the HTF to the channel wall must be obtained solving energy equation using the velocities obtained from the answers of eq. 5. The following is the energy equation for the convective heat transfer process:

$$\rho_f C_{pf} \frac{DT}{Dt} = k_s \nabla^2 T \qquad \text{(eq. 5)}$$

Where C_{pf} is the HTF specific heat, k_s is the thermal conductivity of solid, and T is the temperature. DT/D is the material derivative term in Eq(5). governs the transient response during heat transfer process.

5. Model validation and numerical simulation

Larrinaga et.al. [7] provides a detailed description of the TES design employed in this investigation. The TES module, Case A is validated using same design parameters, material properties, boundary conditions and solver parameters used in authors experimental study. The energy accumulated and released in TES during charging and discharging process is validated with the experimental data reported in their study. The solution domain after validation is further scaled to increase the energy storage capacity for case A and in case B, fins are added to acquire the calculated heat transfer area. The time for discharging and charging of TES module for case A and case B is also calculated analytically using Eq. 8 which proves the validation of CFD results. Fig. 5 shows the energy accumulated and discharge from TES for the parameter used in Larrinaga et.al. [7] study.

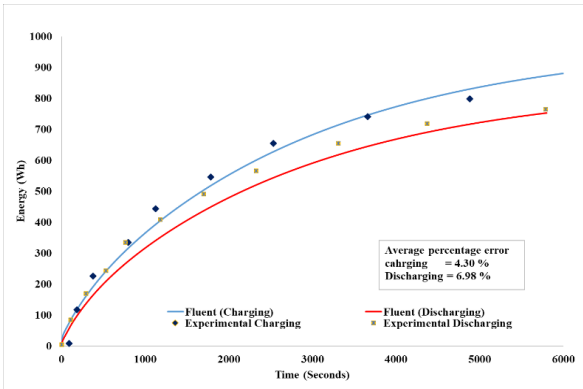

Fig. 5: Energy stored and released for the temperature range (60 - 65°C)

6. Grid independence test

A hybrid mesh is used for the discretization of the domain with an average aspect ratio of 1.1 and skewness of order 10^{-3}. Discharge of TES is computed for four different mesh for the same parameters to determine the optimal size of the element, as shown in Fig.6.

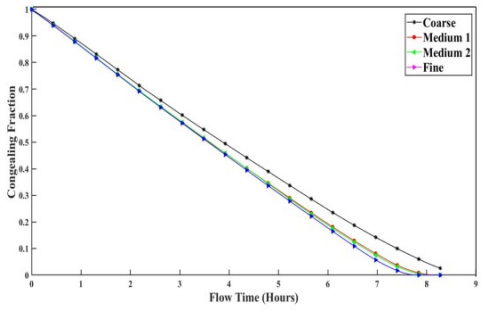

Fig. 6: Solidification Vs. Flow time at mass flow rate 0.11 kg/s

To save the computation time, medium 1 mesh is selected with 234521 elements from Tab. 2. For the optimal mesh size, the influence of the time step was investigated using three different values of 1, 0.1, and 0.5 seconds. The average

PCM liquid fraction changed very slightly when the time step was reduced from 0.5 to 1 second; consequently, the time step of 1 s was considered.

Tab. 2: Mesh details

Mesh Type	No of Elements	No of Nodes
Coarse Mesh	42000	43529
Medium Mesh 1	103500	105797
Medium Mesh 2	216000	219073
Fine Mesh	288000	291097

7. Results and discussion

For the both charging and discharging process the analysis of temperature distribution throughout domain, TES thermal efficiency, energy storage rate and the dryer performance is investigated and reported under this study. The drying quality from SDU integrated with TES is analyzed by comparing the performance assessment parameters for different mass flow rates. Fig. 7 shows the charging and discharging profile of TES system at different mass flow rate. Fig. 8 shows, the temperature contour and the high-temperature HFT near the tube wall in contact with the PCM resulting the phase transition and development of interface separating solid and liquid region separated by mushy zone. The interface propagates in the direction of negative temperature gradient resulting to the generation of wavefront of larger width near the inlet and subsequently shorter away from inlet. Due to addition of fins and large heat transfer area the charging and subsequent discharging is faster as compared to normal case.

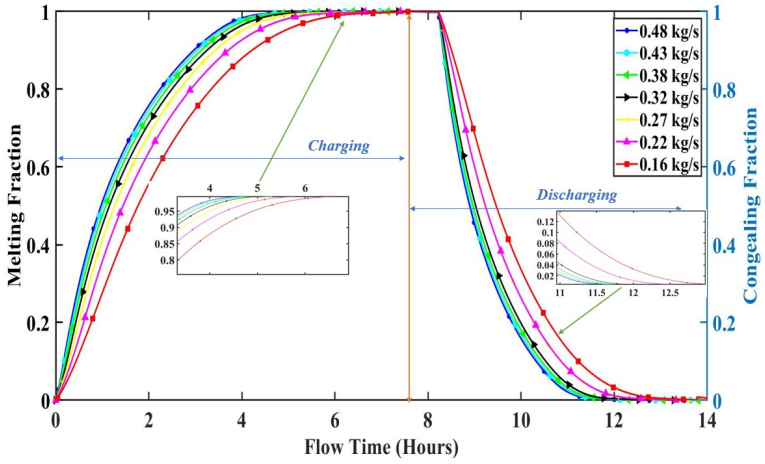

Fig. 7: Melting and solidification profile for Case A

The rate index and the efficiency index are the two most important metrics for evaluating the TES system's performance. Any TES system's efficiency must be calculated using the energy storage rate and discharge rate. The rate of energy storage in TES is computed using equation 4 and shown in figures 8 and the energy discharge and supplied to the dryer can be observed in figure 9. Assuming that the system is started at 150°C, and that the HTF enters the TES unit at 200°C, the higher initial energy transfer rate in figures 8 and figure 9 is due to the large temperature differential which is later steady.

As observed from the Fig 9 and 10, the energy difference gradually decreases and approaches to steady value, due to latent heat absorption of PCM and average temperature of the PCM reaches to its, melting point.

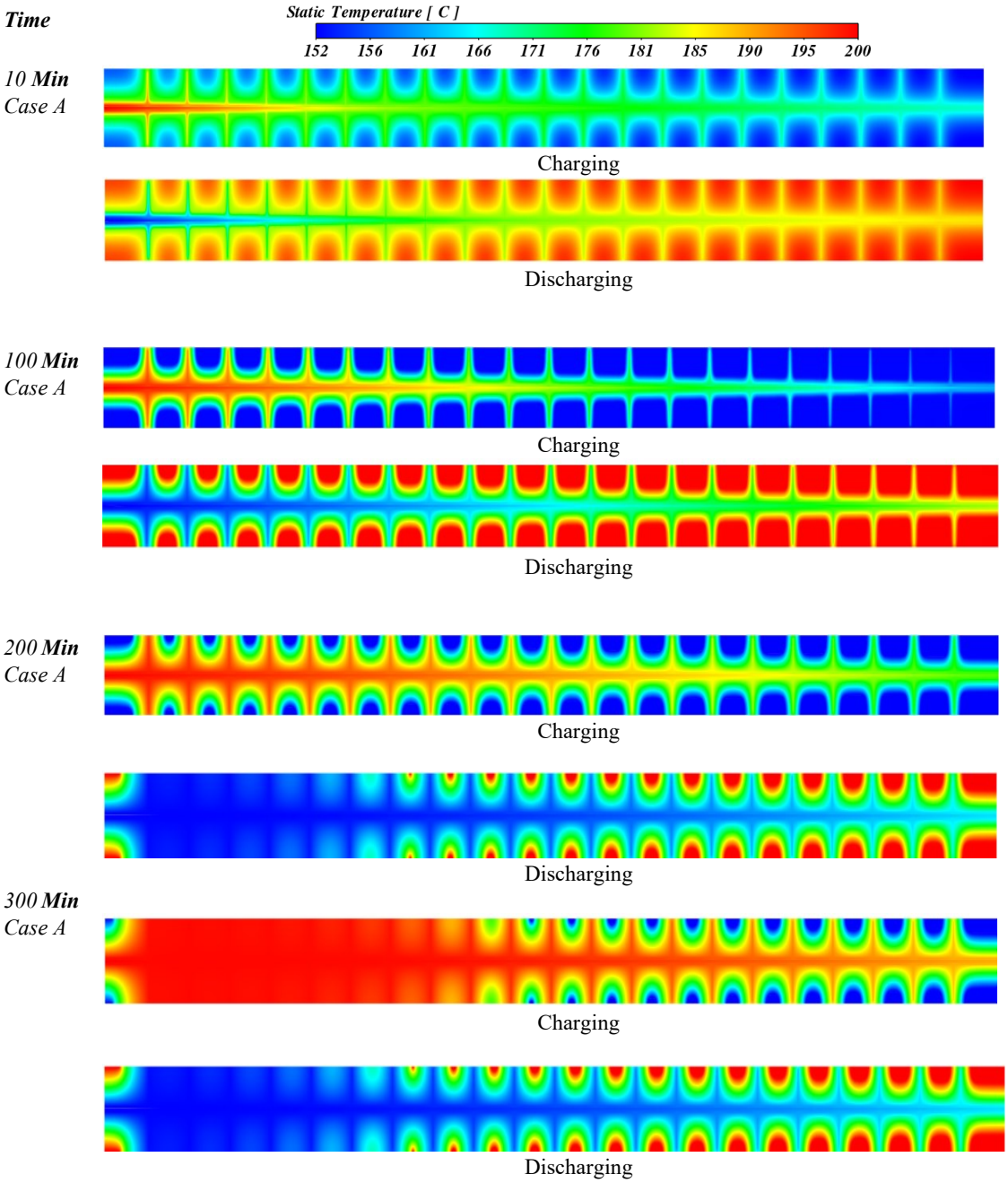

Fig. 8: Temperature contour in case of charging and discharging

It is clear from the observation that latent heat, which is directly related to the liquid volume fraction, dominates the heat storage and release processes due to presence of fin. The results of Fig. 8 shows temperature contour of the TES module with fin have a substantial impact on charging and discharging.

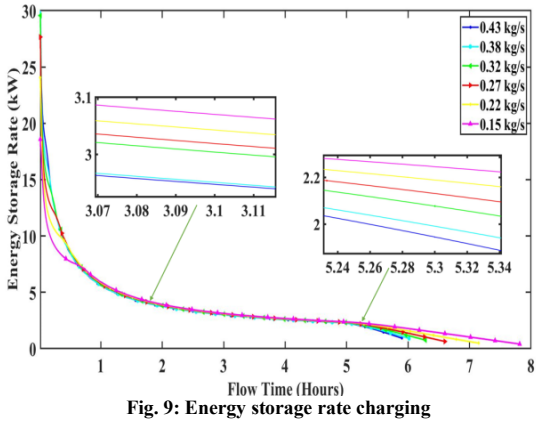

Fig. 9: Energy storage rate charging

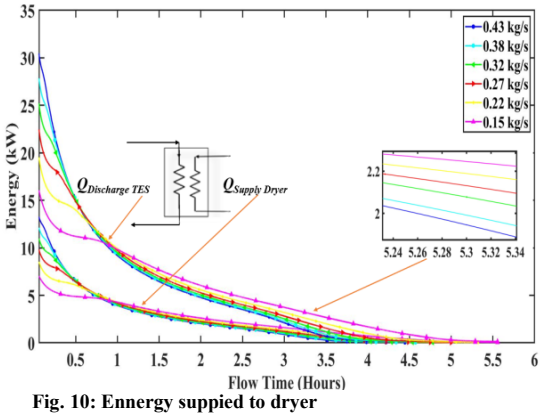

Fig. 10: Ennergy suppied to dryer

The following eq .6 is used to determine the time-averaged Nusselt number.

$$Nu = \frac{1}{\tau}\int_0^{\tau} Nu(\tau)d\tau = \frac{1}{\tau}\int_0^{\tau} \frac{qD_c d\tau}{(T_w - T_m)k_l} \qquad \text{(eq. 6)}$$

The creation of a thin liquid PCM layer near the outside wall of the heat transfer tube causes the Nusselt number to be higher at the beginning of the charging process. The Nusselt number then drops significantly once the heat resistance increases resulting to the growth of the liquid PCM layer. It's also worth noting that around t=0.4, for both the cases the Nusselt number steadily increases, showing that natural convection dominates heat transfer due to the creation of liquid PCM. The Nusselt number begins to rapidly decrease after around t= 0.8, until the charging process is completed. Because most solid PCM is entirely melted to the liquid, the heat transfer method is dominated by conduction, lowering the temperature field variation of the liquid PCM in the TES unit.

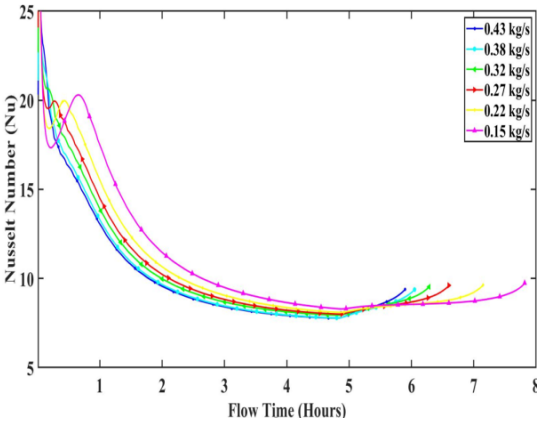

Fig. 11: Nusselt Number Charging

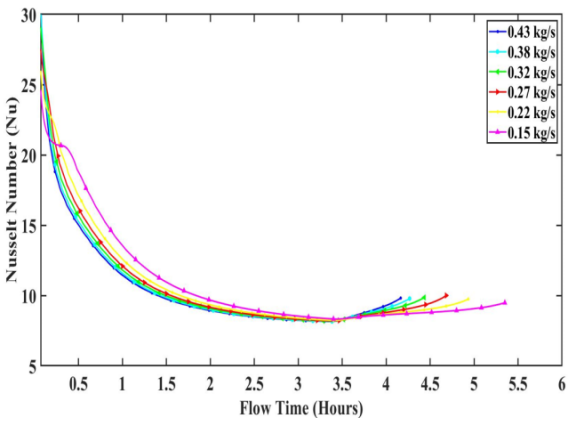

Fig. 12: Nusselt Number Discharging

The average value of Nusselt number observed over the total time duration during discharging is lower than the charging as reported in Fig. 11. The elevation in the Nusselt number curve for different mass flow rate in Fig. 11 and Fig. 12 for charging and discharging respectively is limited due to conduction is dominating and the length of heat transfer process is also greater. The typical charging and discharging inlet temperatures indicate the temperature range in which the TES system will operate. According to the experimental studies[9] conducted earlier the temperature range play a significant role in the thermodynamics and heat transport mechanisms. Fig. 13, shows the temperature profile during charging and discharging for both the case. After gaining sensible heat response of the system is more

stable in comparison during both charging and discharging, due to high uniformity index. However, the rating index and efficiency index is higher.

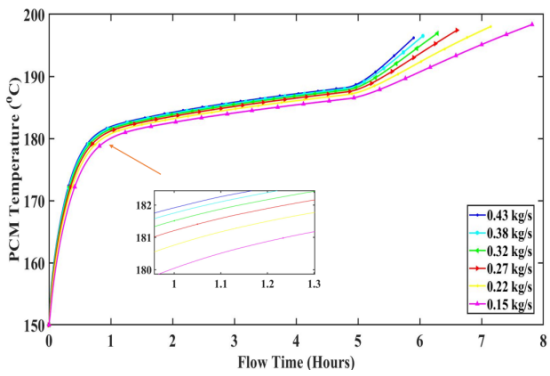

Fig. 13(a): PCM Temperature charging

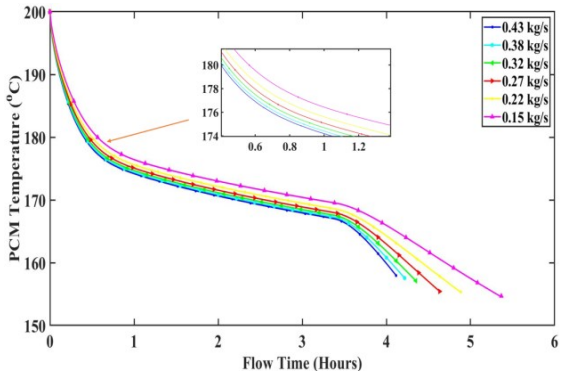

Fig. 13(b): PCM Temperature discharging

Fig. 13: Temperature profile for case A and case B

8. Conclusions

The SDU design integrated with TES for direct drying during sunshine hours and drying in off sunshine hour is proposed in this work. The performance of TES design, is numerically investigated for the different values of mass flow rate. At the lowest value of mass flow rate 0.15 kg/s the SDU performance is comparatively better. The gradient of energy supplied to the drier is less steep provides less variation in supplied energy, as observed from Fig. 9, and the time period of discharge is also increased. During discharge, the high mass flow rates reduce the unit's operational time and dried product quantity due to a sharp increase/decrease in a temperature gradient. The conventional dryer used at a commercial scale consumes either electric energy or energy released from burning fossil fuel or mass to heat air, utilized for drying. The proposed SDU unit for drying 20 kg/batch is worthy of replacing conventional dryers and utilizing renewable energy to reduce carbon and toxic gas emissions.

9. Acknowledgment

This work is conducted under Indo-Australian joint project entitled “Thermal Energy Storage for Food/Grain Drying with CST/RE to Lower Pollution” funded by DST, India

10. References

[1] Mehran S, Nikian M, Ghazi M, Zareiforoush H, Bagheri I., 2019. Experimental investigation and energy analysis of a solar-assisted fluidized-bed dryer including solar water heater and solar-powered infrared lamp for paddy grains drying. Sol Energy, 190, 167–84.

[2] Atalay H. Performance analysis of a solar dryer integrated with the packed bed thermal energy storage (TES) system. Energy 2019., 172, 1037–52.

[3] Lamrani B, Draoui A. Modelling and simulation of a hybrid solar-electrical dryer of wood integrated with latent heat thermal energy storage system. Therm Sci Eng Prog 2020, 18:100545.

[4] Malwad D, Tungikar V. Experimental performance analysis of an improved receiver for Scheffler solar concentrator., 2020. SN Appl Sci, 2.

[5] Therminol 66 Heat Transfer Fluid n.d. https://www.therminol.com/product/71093438.

[6] Crespo A, Barreneche C, Ibarra M, Platzer W. Latent thermal energy storage for solar process heat applications at medium-high temperatures – A review., 2019. Sol Energy, 192, 3–34..

[7] Larrinaga P, Diarce G, Campos-Celador Á, García-Romero A. Parametric characterization of a full-scale plate-based latent heat thermal energy storage system., 2020. Appl Therm Eng;178, 115441.

[8] Ng EY, Johnson PW, Watkins S. An analytical study on heat transfer performance of radiators with non-uniform airflow distribution 2005., 219, 1451–67.

[9] Al-Abidi AA, Mat S, Sopian K, Sulaiman MY, Mohammad AT. Internal and external fin heat transfer enhancement technique for latent heat thermal energy storage in triplex tube heat exchangers. 2013. Appl Therm Eng, 53, 147–56.